[11]The extension of the method to the case where H_A supports a set of three-body bound states is considered in Ref. 5.
[12]R. Sugar and R. Blankenbecler, Phys. Rev. 136, B472 (1964); see also L. Rosenberg, Phys. Rev. D 1, 1019 (1970).
[13]R. S. Christian and J. L. Gammel, Phys. Rev. 91, 100 (1953).
[14]See e.g., J. W. Humberston, Nucl. Phys. 69, 291 (1965); R. Aaron, R. D. Amado, and Y. Y. Yam, Phys. Rev. 140, B1291 (1965).
[15]W. T. H. Van Oers and J. D. Seagrave, Phys. Letters 24B, 562 (1967); J. D. Seagrave and W. T. H. Van Oers, in *Proceedings of the Symposium on Light Nuclei, Few Body Problems, and Nuclear Forces, Bresla, Yugoslavia, 1967* (Gordon and Breach, London, 1968); also a private communication from J. D. Seagrave.
[16]L. M. Delves and A. C. Phillips, Rev. Mod. Phys. 41, 504 (1969).
[17]L. Koester, and H. Ungerer, Z. Physik 219, 300 (1969). The authors are grateful to J. D. Seagrave for making this reference known to them.
[18]J. W. Humberston, Phys. Letters 10, 207 (1964).
[19]T. G. Pett, Phys. Letters 24B, 25 (1967).
[20]None of the potentials used in these calculations are realistic and, as a matter of fact, all substantially overbind the triton. This may account for the low scattering lengths. See, e.g., L. M. Delves and A. C. Phillips, Rev. Mod. Phys. 41, 508 (1969).
[21]This behavior is not unlike lower-bound binding-energy calculations. See, e.g., Ref. 16.
[22]R. N. Madan, Phys. Rev. 173, 214 (1969).

PHYSICAL REVIEW C VOLUME 5, NUMBER 3 MARCH 1972

Isospin-Forbidden Particle Decay of the First $T=\frac{3}{2}$ States in ^{9}Be and ^{9}B

J. C. Adloff, W. K. Lin, K. H. Souw, and P. Chevallier
Centre de Recherches Nucléaires, Université Louis Pasteur, Strasbourg, France
(Received 19 October 1971)

The particle decays of the first $T=\frac{3}{2}$ state in ^{9}Be (^{9}B) have been studied by the ^{7}Li(^{3}He,pn) reaction at $E(^3\text{He})=10.0$ MeV (8.7 and 7.95 MeV). Protons (neutrons) emitted at 0° were detected in coincidence with decay neutrons (protons). Neutron energy was determined by the associated-particle time-of-flight technique. The ratios of partial neutron (proton) widths to the ground and first excited states of ^{8}Be to the ground-state radiative width Γ_{γ_0} are found to be, respectively, 6.4 ± 2.0 and 20.4 ± 4.6 for the ^{9}Be analog state (<1.5 and 13.9 ± 2.1 for ^{9}B). Taking $\Gamma_{\gamma_0}=10.5\pm1.5$ eV, these results give $\Gamma_{n_0}=67\pm26$ eV, $\Gamma_{n_1}=213\pm56$ eV, $\Gamma_{p_0}<18$ eV, and $\Gamma_{p_1}=147\pm30$ eV for the mirror decays.

1. INTRODUCTION

In spite of the isospin selection rule, it has recently been found that the $T=\frac{3}{2}$ states in several $A=4n+1$ nuclei[1-4] decay to $T=0$ low-lying states of the corresponding $A=4n$ nuclei with $Z=N$. The branching ratios of these decays are very charge asymmetric. Since the isospin-forbidden width is a measure of isospin impurity in the analog state, one hopes to obtain information on the charge-dependent effects inside the nucleus from such measurements. Theoretical calculations for $A=13$ by Arima and Yoshida[5] show that the observed partial widths[1] can be qualitatively explained by consideration of isospin mixing due to residual Coulomb interaction within the $1p$-shell configuration states and mixing with the continuum states due to single-particle Coulomb interactions. Presence of a charge-dependent nuclear force is, however, not essential for theoretical-experimental agreement. Recent calculations for the isospin mixing in the first $T=\frac{3}{2}$ states of ^{9}Be and ^{9}B by one of the authors[6] have shown that the residual Coulomb interaction within $1p$-shell configuration states is too small to account for the observed total widths[7] of the analog states. Measurements of the isospin-forbidden particle decays in mass-9 nuclei may be able to give better evidence concerning the existence of a charge-dependent nuclear force.

In the present experiment, the reactions ^{7}Li(^{3}He,p)^{9}Be and ^{7}Li(^{3}He,n)^{9}B were used to populate analog states. The decays were observed by detecting the protons (neutrons) in coincidence with the decay neutrons (protons). The processes in-

duced by ^{3}He bombardment on ^{7}Li are summarized as follows:

$$^7\text{Li} + {}^3\text{He} \rightarrow p + {}^9\text{Be}^* \rightarrow p + n + {}^8\text{Be}^* \rightarrow p + n + 2\alpha \quad (\alpha_1)$$

$$\rightarrow p + \alpha + {}^5\text{He}^* \rightarrow p + n + 2\alpha \quad (\alpha_2)$$

$$\rightarrow n + {}^9\text{B}^* \rightarrow n + p + {}^8\text{Be}^* \rightarrow p + n + 2\alpha \quad (\beta_1)$$

$$\rightarrow n + \alpha + {}^5\text{Li}^* \rightarrow p + n + 2\alpha \quad (\beta_2)$$

$$\rightarrow d + {}^8\text{Be}^* \quad (\gamma)$$

$$\rightarrow t + {}^7\text{Be}^* \quad (\delta)$$

$$\rightarrow \alpha + {}^6\text{Li}^* \quad (\epsilon)$$

$$\rightarrow \text{multiparticle breakup.} \quad (\phi)$$

The asterisks stand for transitions to the ground state, as well as for transitions to excited states. γ decays are not listed. Here we are interested mainly in the (α) and (β) reactions. Those that proceed via the first $T = \frac{3}{2}$ states in ^{9}Be (^{9}B) belong to just one of the many processes leading to the final $p + n + 2\alpha$ state. They compete with all the other reactions including (α) and (β) reactions leading to other excited states. However, the decays of the first $T = \frac{3}{2}$ levels could be identified by the well-defined energy of the ^{7}Li + ^{5}He exit-channel particles, owing to the narrow width of the $T = \frac{3}{2}$ levels.

By detecting protons (neutrons) at 0° the angular correlation of neutrons (protons) from decays of ^{9}Be (^{9}B) excited states is axially symmetric and the well-defined parity of the states ensures that the angular correlation may be expressed as a sum of even-l Legendre polynomials. The spin $\frac{3}{2}$ of the ^{9}Be (^{9}B) first $T = \frac{3}{2}$ state [taken from the spin of ^{9}Li(g.s.)] further eliminates terms higher than $P_2(\cos\theta_{\text{c.m.}})$. Detection of decay particles at $\theta_{\text{c.m.}} = 125°$, a zero of $P_2(\cos\theta_{\text{c.m.}})$, which corresponds to θ_{lab} very close to 120°, eliminates the need to measure the angular correlation in order to determine the branching ratios.

As will be explained in Sec. 2, our measurements gave directly the partial neutron (proton) widths Γ_{n_0} and Γ_{n_1} (Γ_{p_0} and Γ_{p_1}) for decays of the 14.39-MeV (14.67-MeV) state in ^{9}Be (^{9}B) to the ^{8}Be(g.s.) and ^{8}Be(2.9 MeV) states, respectively, as 6.4 ± 2.0 and 20.4 ± 4.6 (<1.5 and 13.9 ± 2.1) in units of the corresponding ground-state radiative width Γ_{γ_0}. As discussed in Ref. 7, we took $\Gamma_{\gamma_0} = 10.5 \pm 1.5$ eV[8] for both the ^{9}Be and ^{9}B analog states, according to the rule that corresponding $\Delta T = \pm 1$ $M1$ γ transitions in conjugate nuclei are identical in all properties.[9] The results are $\Gamma_{n_0} = 67 \pm 26$ eV, $\Gamma_{n_1} = 213 \pm 56$ eV, $\Gamma_{p_0} < 18$ eV, and $\Gamma_{p_1} = 147 \pm 30$ eV for the mirror decays. From the neutron spectrum for decay of ^{9}Be(14.39 MeV), we were also able to deduce a width of 328 ± 110 eV for the α_0-particle decay and possibly the neutron decay to ^{8}Be(11.5 MeV) state.

2. EXPERIMENTAL METHODS

The ^{3}He^{++} beam was obtained from the 5.5-MV

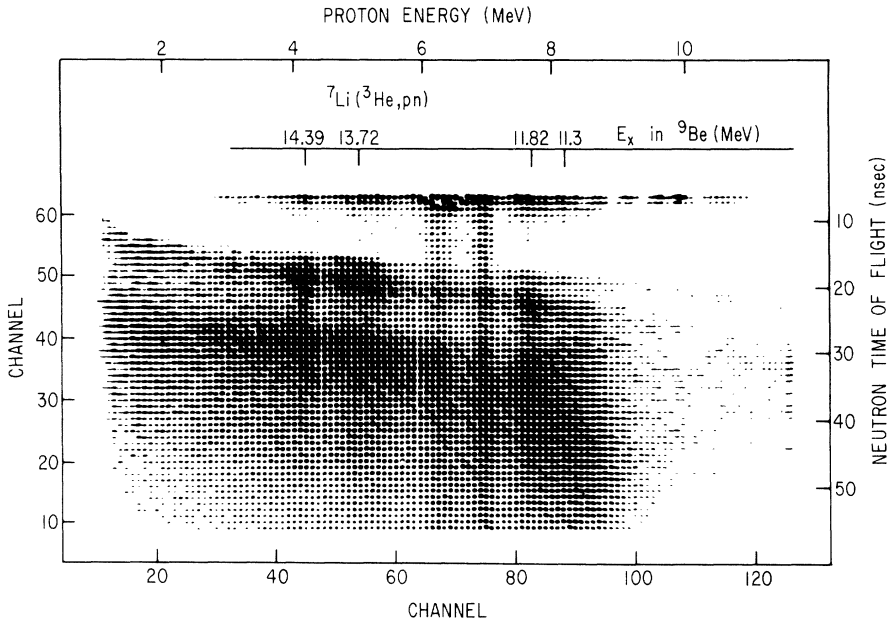

FIG. 1. Neutron time of flight versus proton energy spectrum from ^{7}Li + ^{3}He, $E(^3\text{He}) = 10$ MeV, $\theta_p = 0°$, $\theta_n = 120°$. The flight path is 71.2 cm. The two vertical lines appearing around proton channels 75 and 67 are random lines from the prolific ^{7}Li(^{3}He,t_0) and ^{7}Li(^{3}He,t_1) reactions at 0°. The counts along flight-time channel ~62 come from the tail of particle-γ coincidences.

Van de Graaff accelerator of the Centre de Recherches Nucléaires. The magnetically analyzed beam was collimated to a 2-mm-diam spot. Targets of metallic lithium, enriched to 99.99% in ^{7}Li, were evaporated onto tantalum backings in a separate vacuum system and transferred under vacuum to the target chamber in a specially constructed target holder. Details of the beam, target thickness, detectors, and data handling are described further in individual sections.

A. Decays of the 14.39-MeV State in ^{9}Be

The 14.39-MeV state in ^{9}Be was populated by bombardment of a 10.0-MeV ^{3}He beam on a 220-μg/cm^2 ^{7}Li target. The tantalum target backing (31 μ) was thick enough to range out the incident beam while letting protons pass through into a solid-state detector at 0°. This proton detector (1000 μ thick) was collimated by a 7-mm-diam circular aperture 2.2 cm from the target. As mentioned in Ref. 7, it was difficult to extract the number of protons populating the ^{9}Be(14.39 MeV) state directly from the proton singles spectrum. In order to obtain proper normalization for the p-n coincidence spectrum of this work and the p-γ coincidence spectrum measured in Ref. 7, we used the same monitoring system. It consisted of a 350-μ-thick surface-barrier counter set at −140° to the beam direction, collimated by a 3-mm-diam circular aperture 3.3 cm from the target and covered by 100 μ of aluminum. The deuteron group from the reaction ^{7}Li(^{3}He, d_0)^{8}Be [reaction (γ)] stood out clearly in the monitor spectrum and was used for normalization. The neutron detector, located at 120°, was a 12.7-cm-diam by 5.08-cm-thick Naton 136 plastic scintillator coupled to a 58 AVP photomultiplier. The associated-particle time-of-flight technique was used to determine the neutron energy. The flight path was 71.2 cm. The start pulse for time-to-amplitude convertor was taken through a fast discriminator from the anode of the photomultiplier tube. The stop pulse, also taken through a fast discriminator, was derived from the output of the time-pick-off unit of the proton detector. An Intertechnique 8192-channel analyzer operating in a two-dimensional mode was used to store neutron flight time versus proton energy. The analyzer was gated by dynode pulses through a slow discriminator whose threshold was set at 450-keV neutron energy.

Figure 1 shows the two-dimensional spectrum which resulted from a 30-h measurement with a beam intensity of 30 nA. The decays of the ^{9}Be (14.39 MeV) state appear around proton channel 45, above the background coming from decays of broad low-lying states in ^{9}B [reaction (β_1)]. Because the protons populating the 14.39-MeV state have a well-defined energy, as shown in Fig. 2, it was possible to separate out its decay from the others by examining the coincident proton spectrum for fixed flight time, channel by channel. The results corrected for random events are shown in Fig. 3. The dashed curves are the spectral shapes calculated for various decay modes. In these calculations, a generalized density-of-states func-

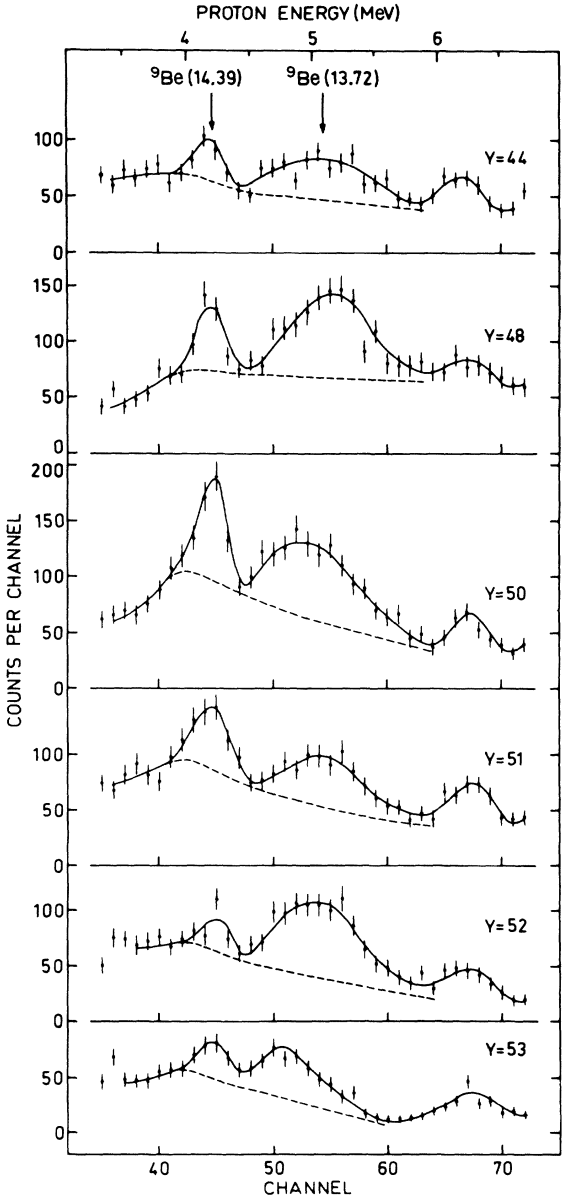

FIG. 2. Sample of partial proton spectra corresponding to six time-of-flight channels (Y) of Fig. 1 as indicated by the channel numbers. The dashed lines represent the assumed background in extracting the yield per time-of-flight channel for the ^{9}Be(14.39 MeV) and ^{9}Be(13.72 MeV) decays.

tion[10] was used to represent the neutron energy spectrum in the center-of-mass system of the decaying ^{9}Be. The parameters involved are shown in Table I.[10-14] For the n-α channel, we used directly the phase shifts calculated by Tombrello.[14] The finite solid angles of the detectors, as well as the efficiency of the neutron detector, were considered in the transformation of the spectrum to laboratory system. The flight-time response function for monoenergetic neutrons was taken from the shape for t-γ coincidences of the reaction ^{7}Li-(^{3}He, t_1)^{7}Be$^*(\gamma)^7$Be [reaction (δ)]. Appearing in higher flight-time channels, part of this shape is visible in Fig. 1.

Decay of the ^{9}Be(14.39 MeV) state to ^{8}Be(11.5 MeV) [reaction (α_1)] corresponding to an f-wave neutron emission, is expected to be weak. A least-squares fit to the experimental neutron spectrum gives preference for the decay mode ^{9}Be(14.39 MeV)(α)^{5}He(n)^{4}He [reaction (α_2)] over the decay to ^{8}Be(11.5 MeV). The best fit (solid curve of Fig. 2) was obtained by including only the neutron decays to ^{8}Be(g.s.), ^{8}Be(2.9 MeV), and the α-particle decay. We deduced from this fit the number of p-n coincidences, N_{pn}, corresponding to each of these decay modes. The ratio of each partial width Γ_n to the ground-state radiative width Γ_{γ_0} is given by

$$\frac{\Gamma_n}{\Gamma_{\gamma_0}}=\frac{4\pi N_{pn}/f_n\epsilon_n\Delta\Omega_n}{N_{p\gamma_0}/(\epsilon\Delta\Omega)_{\gamma_0}}\times\frac{N_d'\Delta\Omega_p'}{N_d\Delta\Omega_p}, \quad (1)$$

where ϵ_n and $\Delta\Omega_n$ are, respectively, the mean efficiency and solid angle of the neutron detector. The quantity $f_n\Delta\Omega_n$ is the solid angle appearing in the center-of-mass system of decaying ^{9}Be. N_d is the number of monitor deuteron counts. $\Delta\Omega_p$ is the solid angle subtended by the proton detector. The corresponding N_d' and $\Delta\Omega_p'$ have the same meanings, but they were measured in the p-γ coincidence experiment described in Ref. 7. The ratio $N_{p\gamma_0}/(\epsilon\Delta\Omega)_{\gamma_0}$, taken from this experiment [also at $E(^3\text{He})=10.0$ MeV)], is the number of p-γ_0 coincidences divided by the total absolute efficiency of the γ-ray detector. The second factor in expression (1) accounts for the difference in proton-detector solid angle, target thickness, and integrated charge. The computed results are $\Gamma_{n_0}/\Gamma_{\gamma_0}=6.40\pm2.0$, $\Gamma_{n_1}/\Gamma_{\gamma_0}=20.4\pm4.6$, and $\Gamma_{\alpha_0}/\Gamma_{\gamma_0}=31.2\pm9.8$. Finally, when combined with $\Gamma_{\gamma_0}=10.5\pm1.5$ eV,[8] these ratios yield $\Gamma_{n_0}=67\pm26$ eV, $\Gamma_{n_1}=213\pm56$ eV, and $\Gamma_{\alpha_0}=328\pm110$ eV.

B. Decays of the 14.67-MeV State in ^{9}B

The technique used to measure the ^{9}B(14.67 MeV) decays was similar to that used for the ^{9}Be (14.39 MeV) decays, the role of the neutron and proton counter being interchanged. A ^{7}Li target (180 μg/cm^2 thick) was evaporated on a 31-μ tantalum backing. The proton detector (2000 μ thick) was collimated by a 2×7-mm rectangular aperture 3 cm from the target and was covered by a 25-μ tantalum foil. Again the same monitoring system was used to detect the deuteron from the reaction ^{7}Li(^{3}He, d_0)^{8}Be. Measurement of this deuteron group allowed straightforward normalization for the n-p coincidence spectrum and the n-γ coincidence spectrum measured in Ref. 7. The result of a 31-h measurement with a beam intensity of 100 nA at $E(^3\text{He})=8.7$ MeV is shown in Fig. 4. Proton decays from the ^{9}B(14.67 MeV) state lie horizontally around flight-time channel 20. The decay to the broad ^{8}Be(2.9 MeV) state clearly appears around proton energy channel 76, but that to

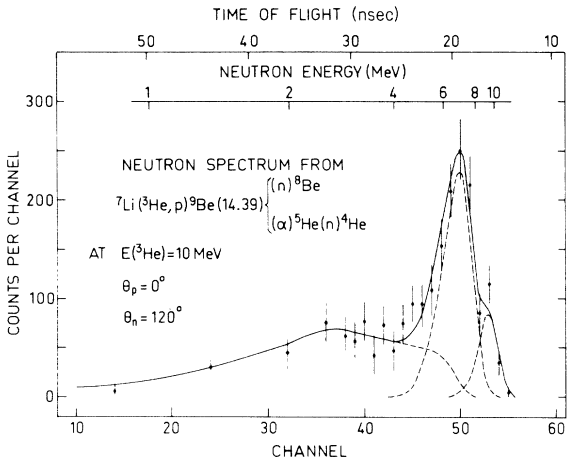

FIG. 3. Neutron time-of-flight spectrum obtained for the ^{9}Be(14.39 MeV) decays. The experimental points higher than channel 37 were obtained from the corresponding proton spectra, some of which are shown in Fig. 2. The four points below channel 38 were obtained by averaging the yield extracted from proton spectra projected between flight-time channels 35–37, 29–34, 19–28, and 9–18. The peaks (dashed lines) centered at flight-time channels 53, 50, and the broad structure around channel 36, represent, respectively, the calculated spectral shapes for the decays to ^{8}Be(g.s.), ^{8}Be(2.9 MeV), and ^{5}He(g.s.).

TABLE I. Parameters used in calculating spectral shapes for the decay of ^{9}Be(14.39 MeV).

Channel	Radius (fm)	l	E_R (MeV)	γ^2 (MeV)	Refs.
α-α	3.5	0	0.096	4.28	10
	3.5	2	3.28	3.36	11
	4.4	4	11.5	2.11	12
n-^{8}Be	4.35	1			13
n-α		1			14
α-^{5}He	4.35	0			

^{8}Be(g.s.) falls too close to the intense decay from ^{9}Be(2.43 MeV)$(n)^8$Be(2.9 MeV) [reaction (α_1)]. Most of the counts lying below proton channel 90 on the ^{8}Be(g.s.) and ^{8}Be(2.9 MeV) kinematic lines are expected to come from neutron decays[13] of ^{9}Be(4.7 MeV) and ^{9}Be(6.8 MeV) [reaction (α_1)], and also from ^{7}Li(^{3}He, $n)^9$B$(p)^8$Be via the 11.62- and 12.06-MeV states in ^{9}B [reaction (β_1)]. As will be seen later, the neutron decay of the 6.8-MeV state ($\Gamma \sim 1.3$ MeV) in ^{9}Be to the broad ^{8}Be (2.9 MeV) state is responsible for the increase in yield here around proton channel 60. By using expression (1) with n and p interchanged, we deduce $\Gamma_{p_1}/\Gamma_{\gamma_0} = 15.2 \pm 2.3$ for the proton decay of ^{9}B(14.67 MeV) to the ^{8}Be(2.9 MeV) state.

Hoping to obtain a better separation between the decay from ^{9}B(14.67 MeV)$(p)^8$Be(g.s.) and that from ^{9}Be(2.43 MeV)$(n)^8$Be(2.9 MeV), a measurement at $E(^3\text{He}) = 7.95$ MeV was undertaken. By lowering the bombarding energy, the decreases in both the neutron energy from ^{7}Li(^{3}He, $n)^9$B(14.67 MeV) and the proton energy from ^{7}Li(^{3}He, p)-^{9}Be(2.43 MeV) have made the separation possible, as can be seen in Fig. 6. In order to extract the ratios $\Gamma_p/\Gamma_{\gamma_0}$ at this new bombarding energy, we chose to measure both the γ-ray and proton decays of the ^{9}B(14.67 MeV) state simultaneously. This has the advantages of eliminating the ^{7}Li-(^{3}He, $d_0)^8$Be normalizing measurement, as well as the geometric and neutron-efficiency corrections for the neutron detector. Instead of expression (1), the ratios $\Gamma_p/\Gamma_{\gamma_0}$ are related in a simpler way to the measured coincidence yields as

$$\frac{\Gamma_p}{\Gamma_{\gamma_0}} = \frac{4\pi N_{pn}/(f\Delta\Omega)_p}{N_{n\gamma_0}/(\epsilon\Delta\Omega)_{\gamma_0}}. \tag{2}$$

The decay γ rays were detected by a 12.7×10.16-cm NaI crystal mounted on an XP 1040 photomultiplier tube. The distance from the front face of crystal to the target was 7.6 cm. A two-dimensional 4096-channel analyzer was used to record neutron flight time versus energy of the coincident γ ray. The same neutron fast pulses used to start the n-γ time-to-amplitude convertor (TAC) were used as stop pulses for the n-p TAC. Both the 4096-channel analyzer and the 8192-channel analyzer, in which the n-p coincidences were recorded, were gated by the same neutron slow discriminator outputs. The threshold of the discriminator was set at 350 keV in neutron energy. The high-energy portion of the γ-ray spectrum, projected from the corresponding neutron flight time versus γ-ray energy spectrum, is shown in Fig. 5. The γ transitions from the 14.67-MeV state to the ground and 2.33-MeV states contribute peaks centered at channels 111 and 90, respec-

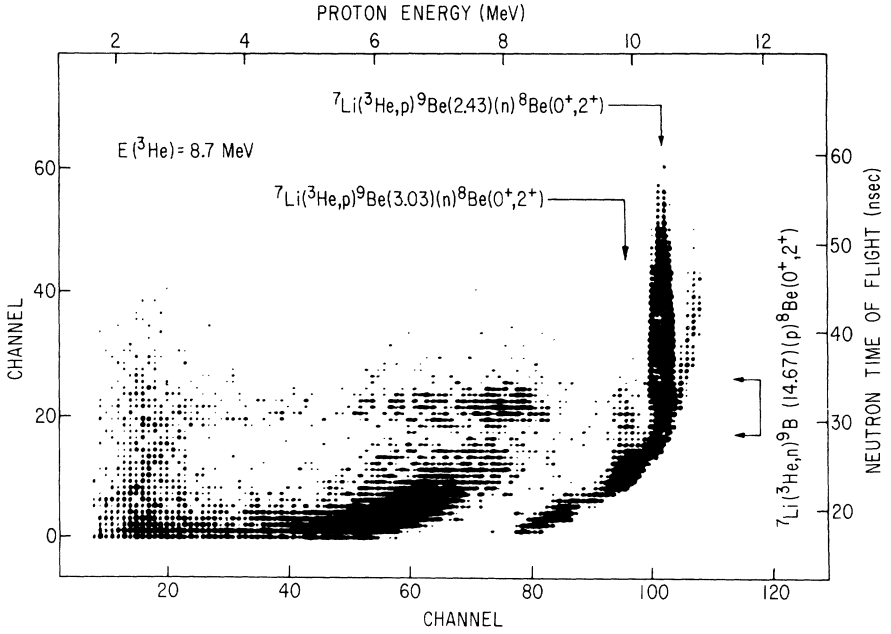

FIG. 4. Neutron time-of-flight versus proton energy spectrum from ^{7}Li + ^{3}He, $E(^3\text{He}) = 8.7$ MeV, $\theta_n = 0°$, $\theta_p = 120°$. The proton counter is covered by a 25-μ tantalum foil. The flight path is 60.1 cm. The ^{8}Be(g.s.) and ^{8}Be(2.9 MeV) kinematic lines are in evidence. The decays of the ^{9}Be(2.43 MeV) and ^{9}Be(3.03 MeV) states to the tail of the broad ^{8}Be(2.9 MeV) state appear as vertical lines. The ^{9}B(14.67 MeV) decays appear in the horizontal region centered around flight-time channel 20. The ^{9}B(14.67 MeV)$(p)^8$Be(g.s.) decay could not be clearly separated from the ^{9}Be(2.43 MeV)$(n)^8$Be(2.9 MeV) decay in this spectrum.

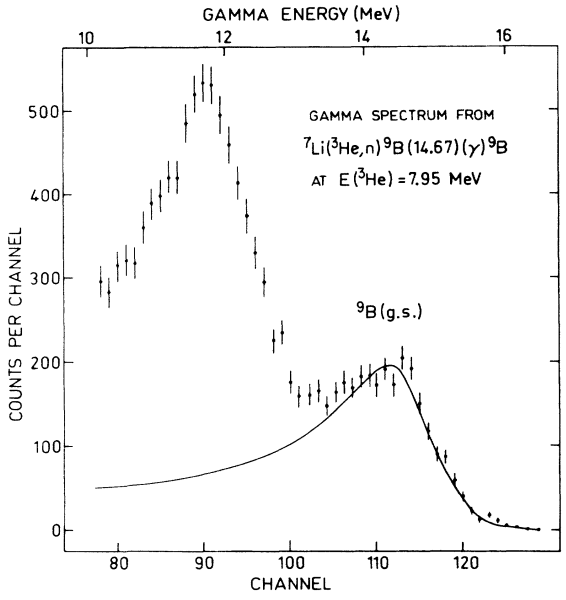

FIG. 5. High-energy portion of a summed γ spectrum from the decays of the ^{9}B(14.67 MeV) state. The n-γ coincidence spectrum, from which this projection was obtained, was taken simultaneously with the coincidence spectrum shown in Fig. 6.

tively. The area under the solid curve represents the ground-state transition. Details on obtaining the n-γ_0 coincidence yield have been given in Ref. 7. In Fig. 6, we display the neutron flight time versus proton energy spectrum obtained in a 26-h measurement with a beam current of 80 nA. The proton decays of the ^{9}B(14.67 MeV) state appear horizontally around flight-time channel 35. A projection between proton channels 54 and 87 onto the flight-time axis is shown in Fig. 7(a). By choosing these limits for the proton energies, the peak centered around flight-time channel 35 contains at least 90% of the coincidence counts coming from the ^{9}B(14.67 MeV)$(p)^8$Be(2.9 MeV) decay. A smooth background was assumed (dashed line). A further check on the background was done by the neutron time-of-flight spectrum projected on the proton-energy axis as shown in Fig. 8. Figure 8(b) shows the proton spectrum in coincidence with neutrons limited by flight-time channel 31 to 41 of Fig. 6. The background (dashed line) was obtained by averaging two proton spectra projected between flight-time channels 25–30 and 42–47 of Fig. 6. The two broad peaks, around channel 62 and 78, appearing in the dashed line, appear also in these two projected proton spectra. These broad peaks come, respectively, from neutron decays of the 6.8- and 4.7-MeV state of ^{9}Be to the ^{8}Be(2.9 MeV) state [reaction (α_1)] and possibly also from the proton decays of the broad 11.62-, 12.06-, and 14.7-MeV states in ^{9}B [reaction (β_1)]. Figure 8(c) shows the proton energy spectrum for the ^{9}B(14.67 MeV)$(p)^8$Be(2.9 MeV) decay after background and random-event subtraction. Figure 8(a) shows the direct proton singles spectrum. Using the coincidence counts N_{np} and $N_{n\gamma_0}$ obtained,

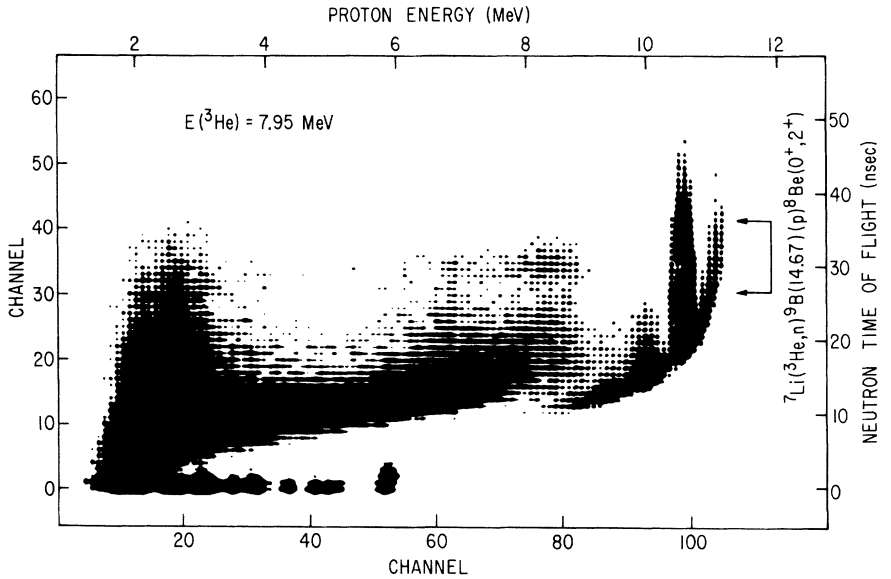

FIG. 6. Neutron time-of-flight versus proton energy spectrum from ^{7}Li + ^{3}He, $E(^3\text{He}) = 7.95$ MeV, $\theta_n = 0°$, $\theta_p = 120°$. The proton counter is covered by a 50-μ aluminium foil. The flight path is 39.8 cm. The counts along flight-time channel ~1 are particle-γ coincidences. The ^{9}B(14.67 MeV)$(p)^8$Be(g.s.) decay on the ^{8}Be(g.s.) kinematic line is now clearly separated from ^{9}Be(2.43 MeV)$(n)^8$Be(2.9 MeV) decay.

respectively, from Figs. 8(c) and 5, expression (2) gives $\Gamma_{p_1}/\Gamma_{\gamma_0} = 12.8 \pm 2.0$. We took the average of this ratio and the one measured with 8.7-MeV bombarding energy, 13.9 ± 2.1, as our final result. Assuming $\Gamma_{\gamma_0} = 10.5 \pm 1.5$ eV we obtained $\Gamma_{p_1} = 147 \pm 30$ eV, in good agreement with the corresponding value given in Ref. 4. Although we were able to obtain a better kinematic separation between decays of ^{9}B(14.67 MeV)$(p)^8$Be(g.s.) and ^{9}Be(2.43 MeV)$(n)^8$Be(2.9 MeV) by lowering the bombarding energy to 7.95 MeV, we were still not able to give a value for the ratio $\Gamma_{p_0}/\Gamma_{\gamma_0}$. The proton decay to ^{8}Be(g.s.) appears to be very weak as compared with that to the ^{8}Be(2.9 MeV) state. Figure 7(b) shows a time-of-flight spectrum, projected along the ^{8}Be(g.s.) kinematic line. By assuming the dashed background, the dash-dot curve drawn on top would give a ratio of 1.5 for $\Gamma_{p_0}/\Gamma_{\gamma_0}$. We took this value as an upper limit, which corresponds to $\Gamma_{p_0} < 18$ eV. The same ground-state radiative width was assumed. Table II summarizes the experimental results obtained in this work.

3. DISCUSSION

Isospin mixing in the first $T = \frac{3}{2}$ states in ^{9}Be and ^{9}B have been discussed, in connection with the observed deviation[15-18] from the quadratic mass formula for the isobaric quartet, by Jänecke[19] and Hardy *et al.*[20] The latter authors have observed, from the reactions ^{11}B$(p, {}^3$He$)^9$Be and ^{11}B$(p, t)^9$B, several $T = \frac{1}{2}$ states near the analog states. These new states have J^π consistent with a $\frac{3}{2}^-$ assignment using the distorted-wave Born-approximation calculations with $1p$-shell wave functions. Difficulties in explaining both the widths of analog states and the d coefficient of the mass formula $M(T_z) = a + bT_z + cT_z^2 + dT_z^3$ have been encountered when a two-state mixing between the analog state and each of these new $T = \frac{1}{2}$ states was assumed. However, as indicated by a model calculation of

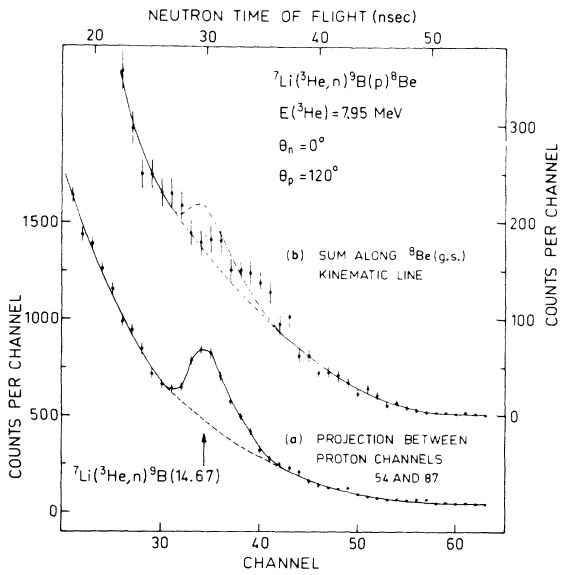

FIG. 7. (a) Partial neutron time-of-flight spectrum projected from the spectrum shown in Fig. 6, between proton channel $X = 54$ and $X = 87$. The assumed background under the ^{7}Li(^{3}He,$n)^9$B(14.67 MeV)$(p)^8$Be(2.9 MeV) decay is shown by the dashed line. (b) Partial neutron time-of-flight spectrum obtained by the summation along ^{8}Be(g.s.) kinematic line from spectrum of Fig. 6. The dashed-dotted curve would give a ratio of $\Gamma_{p_0}/\Gamma_{\gamma_0} = 1.5$, taking the background shown by the dashed curve.

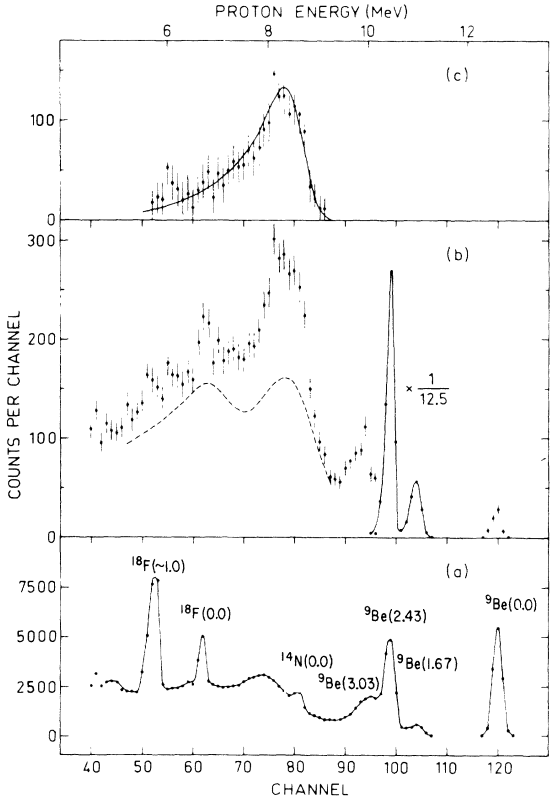

FIG. 8. (a) Partial proton singles spectrum from ^{7}Li + ^{3}He, $E(^3\text{He}) = 7.95$ MeV, $\theta_p = 120°$. The proton groups labeled by ^{14}N and ^{18}F are from ^{12}C$(^3$He, $p)^{14}$N and ^{16}O-$(^3$He, $p)^{18}$F, carbon and oxygen being target contaminants. (b) Partial proton spectrum as the result of the projection from spectrum of Fig. 6 between flight-time channels $Y = 31$ and $Y = 41$. The method of obtaining the background (dashed line) is explained in the text. The main contribution in the peak appearing at channel 104 is expected to come from ^{9}Be(1.67 MeV)$(n)^8$Be(g.s.) decay. The peak at channel 120 is pure random. The broad structure around channel 78 is attributed to the ^{9}B(14.67 MeV)$(p)^8$Be(2.9 MeV) decay. (c) The energy spectrum of decay protons from ^{9}Be(14.67 MeV)$(p)^9$Be(2.9 MeV). The background as indicated in (b) and sharp random peaks around channels 52 and 62 were subtracted. The smooth curve is drawn through data points.

TABLE II. Properties of the first $T=\frac{3}{2}$ states in ^{9}Be and ^{9}B.

^{9}Be		^{9}B	
Γ_{tot} (eV)	500 ± 100 [a]	Γ_{tot} (eV)	400^{+140}_{-180} [a]
Γ_{γ_0} (eV)	10.5 ± 1.5 [b]		
$\Gamma_{n_0}/\Gamma_{\gamma_0}$	6.4 ± 2.0	$\Gamma_{p_0}/\Gamma_{\gamma_0}$	<1.5
$\Gamma_{n_1}/\Gamma_{\gamma_0}$	20.4 ± 4.6	$\Gamma_{p_1}/\Gamma_{\gamma_0}$	13.9 ± 2.1
$\Gamma_{\alpha_0}/\Gamma_{\gamma_0}$	31.2 ± 9.8		
Γ_{n_0} (eV)	67 ± 26 [c]	Γ_{p_0} (eV)	<18 [c]
Γ_{n_1} (eV)	213 ± 56 [c]	Γ_{p_1} (eV)	147 ± 30 [c]
Γ_{α_0} (eV)	328 ± 110 [c]		

[a] Reference 7.
[b] Reference 8.
[c] Our results assuming $\Gamma_{\gamma_0} = 10.5 \pm 1.5$ eV for both ^{9}Be(14.39 MeV) and ^{9}B(14.67 MeV).

TABLE III. Summary of branching ratios (BR) for nucleon decays of $T=\frac{3}{2}$ levels in $4n+1$ nuclei.

	BR (g.s.)	BR (1st ex.s.)	Refs.
^{9}Be	0.13 ± 0.05 [a]	0.43 ± 0.14 [a]	This work
^{9}B	<0.08 [b]	$0.37^{+0.18}_{-0.15}$ [b]	This work
	0.025 ± 0.015	0.33 ± 0.09	4
^{13}C	0.065 ± 0.014	0.250 ± 0.036	1
^{13}N	0.202 ± 0.02	0.121 ± 0.015	1
^{17}O	0.91 ± 0.15	0.05 ± 0.02	2
^{17}F	0.088 ± 0.016	0.23 ± 0.05	2
^{21}Ne	0.55 ± 0.04	0.33 ± 0.03	3
^{21}Na	0.80 ± 0.08	0.17 ± 0.08	3

[a] Our results assuming $\Gamma_{tot}(^9\text{Be}) = 500 \pm 100$ eV.
[b] Our results assuming $\Gamma_{tot}(^9\text{B}) = 400^{+140}_{-180}$ eV.

Mosher, Kavanagh, and Tombrello,[18] the difficulties are not so significant, as deviation from the quadratic mass formula could be explained by a Thomas-Ehrman shift. In probing the charge-dependent effects, it might be more fruitful to proceed with studies of the widths of analog states and their decay modes.

Using the intermediate-coupling shell-model wave functions of Barker,[21] one of the authors[6] has calculated the isospin mixing in the first $T=\frac{3}{2}$ states in ^{9}Be and ^{9}B. It is found that the Coulomb interaction between these configuration states could only account for few percent of the observed partial nucleon widths. Since this could suggest that the effect of a charge-dependence force may be important, an attempt was made to include a charge-dependent nuclear force using the expression given in Ref. 5. This consists of an isovector and an isotensor force. It appears from the calculation that a stronger triplet isotensor force is required in order to bring the calculated partial widths to the right order of magnitude for the observed values.

As pointed out by Adelberger *et al.*,[1] an asymmetry in the ratios of reduced widths for the mirror decays would indicate that the isospin impurity arises from the admixture of more than one state. For the mass-9 decays, we first remove the charge-dependent effect due to differences in penetration factors. Assuming a p-wave nucleon decay with a channel radius of 4.35 fm, the ratios of reduced widths are found to be $\theta_{n_0}^2/\theta_{n_1}^2 = 0.27 \pm 0.10$ and $\theta_{p_0}^2/\theta_{p_1}^2 < 0.12$. Taking the branching ratio for the ^{9}B decay from Ref. 4, the same correction for penetration factors gives $\theta_{p_0}^2/\theta_{p_1}^2 = 0.07 \pm 0.04$. There is still appreciable asymmetry, although it is quite different in nature as compared with those found in other mirror decays. In Table III, we show the branching ratios of these decays in the nuclei studied so far. The asymmetries for both mass-9 and mass-21 decays are smaller, so that one could not really say that this effect is only large for light nuclei as suggested by Cameron, Nielson, and Sharma.[3] It would be interesting if one could analyze those results together and understand why the asymmetry changes so much across this mass region. The calculation of Arima and Yoshida[5] for mass-13 decays has shown that the branching ratios are also sensitive to the exchange character of the charge-independent nuclear force. The analysis therefore might also serve as a test on the consistency of the choice of exchange mixture for the nuclear forces.

ACKNOWLEDGMENTS

We would like to thank Dr. C. L. Cocke, Dr. F. Scheibling, and Dr. Y. Wolfson for helpful discussions. One of us (W.K.L.) wishes to express sincere thanks to Professor P. Chevallier for giving him the opportunity of working at the Centre de Recherches Nucléaires.

[1] E. G. Adelberger, C. L. Cocke, C. N. Davids, and A. B. McDonald, Phys. Rev. Letters 22, 352 (1969).
[2] A. B. McDonald, E. G. Adelberger, H. B. Mak, D. Asherry, A. P. Shukla, C. L. Cocke, and C. N. Davids, Phys. Letters 31B, 119 (1970).
[3] J. M. Cameron, G. C. Neilson, and T. C. Sharma, Phys. Letters 36B, 35 (1971).
[4] E. G. Adelberger, A. B. McDonald, H. B. Mak, A. P. Shukla, and A. V. Nero, Bull. Am. Phys. Soc. 16, 829 (1971).
[5] A. Arima and S. Yoshida, Nucl. Phys. A161, 492 (1971).
[6] W. K. Lin, Phys. Letters 37B, 480 (1971).
[7] J. C. Adloff, K. H. Souw, and C. L. Cocke, Phys. Rev.

C 3, 1808 (1971).
[8]H. G. Clerc, K. J. Wetzel, and E. Spamer, Phys. Letters 20, 667 (1966).
[9]E. K. Warburton and J. Weneser, in *Isospin in Nuclear Physics*, edited by D. H. Wilkinson (North-Holland, Amsterdam, 1969), p. 173.
[10]F. C. Barker and P. B. Treacy, Nucl. Phys. 38, 33 (1962).
[11]T. A. Tombrello and L. S. Senhouse, Phys. Rev. 129, 2252 (1963).
[12]R. Nilson, W. K. Jentschke, G. R. Briggs, R. O. Kerman, and J. N. Snyder, Phys. Rev. 109, 850 (1958).
[13]C. L. Cocke and P. R. Christensen, Nucl. Phys. A111, 623 (1968).
[14]T. A. Tombrello, Phys. Letters 23, 134 (1966).
[15]C. A. Barnes, E. G. Adelberger, D. C. Hensley, and A. B. McDonald, in *Proceedings of the International Conference on Nuclear Physics, Gatlinburg, Tennessee, 12–17 September 1966*, edited by R. L. Becker and A. Zucker (Academic, New York, 1967), p. 261.
[16]P. H. Nettles, D. C. Hensley, and T. A. Tombrello, in *Proceedings of the Second Conference on Nuclear Isospin, Asilomar–Pacific Grove, California, March 1969*, edited by J. D. Anderson, S. D. Bloom, J. Cerny, and W. W. True (Academic, New York, 1969), p. 819.
[17]G. F. Trentelman, B. M. Preedom, and E. Kashy, Phys. Rev. Letters 25, 530 (1970).
[18]J. M. Mosher, R. W. Kavanagh, and T. A. Tombrello, Phys. Rev. C 3, 438 (1971).
[19]J. Jänecke, Nucl. Phys. A128, 632 (1969).
[20]J. C. Hardy, J. M. Loiseaux, J. Cerny, and G. T. Garvey, Nucl. Phys. A162, 552 (1971).
[21]F. C. Barker, Nucl. Phys. 83, 418 (1966).

PHYSICAL REVIEW C VOLUME 5, NUMBER 3 MARCH 1972

Coulomb Correction in Nuclear β Decay: Elementary-Particle Treatment

Lloyd Armstrong, Jr.,* and C. W. Kim†
Department of Physics, The Johns Hopkins University, Baltimore, Maryland 21218
(Received 21 October 1971)

The "elementary-particle" treatment of nuclear β decay is extended to include the effects of final-state Coulomb interactions. The resulting formalism is valid for both allowed and forbidden decays. The Coulomb correction in allowed transitions is considered in detail and compared with the usual impulse-approximation calculation. The spectrum shape factor for the transition $B^{12} \rightarrow C^{12} + e^- + \bar{\nu}_e$ is evaluated as an example.

I. INTRODUCTION

In the "elementary-particle" treatment of nuclear β decay,[1] initial and final nuclei are treated as elementary, rather than composite, particles. The composite nature of the nucleus, which is usually taken into account through the use of a model-inspired nuclear wave function, manifests itself in the elementary-particle treatment through nuclear form factors. The present elementary-particle approach does not, however, include a systematic formulation of the Coulomb correction. Thus, this approach is limited to the treatment of β decay of light nuclei where Coulomb corrections, which are of order αZ, can be neglected. Of course, even for light nuclei, high-accuracy analyses of β-decay spectra such as those required to test the conserved-vector-current (CVC) hypothesis or the existence of second-class currents require knowledge of the Coulomb correction.

In this paper, we extend the applicability of the elementary-particle treatment of nuclear β decay by including the Coulomb correction in the basic formulation. We define the Coulomb correction as the one due to the static Coulomb final-state interaction between the emitted electron (or positron) and the final nucleus. In the nuclear case this is the dominant electromagnetic correction.

In the customary impulse approximation, the Coulomb correction is introduced by replacing the plane-wave electron wave function by the Coulomb-distorted wave function, properly averaged over the initial and final nuclear wave functions.[2-4] Hence, the Coulomb correction in this approximation is, strictly speaking, model-dependent, though in practice some approximations are used to make it model-independent in order to simplify the calculation.

In the elementary-particle treatment the initial and final states are described in terms of form factors or structure functions characteristic of the nuclei as a whole, the numerical values of these form factors reflecting the complexity of the internal nuclear structure. Thus, the form factors play roles of nuclear wave functions and the Coulomb-distorted electron wave function is averaged over the nuclear form factors. The form factors can be obtained directly from the corresponding electron scattering data with the help of the CVC hypothesis. Hence, a model-indepent calculation of the Coulomb correction to high accuracy is, in principle, possible when this